Effect of filler properties on the hydrothermal ageing of bituminous mastics

Varveri, Aikaterini; Jing, Ruxin; Tarsi, Giulia ; Erkens, Sandra

DOI
10.1080/14680629.2021.1903975

Publication date
2021

Document Version
Final published version

Published in
Road Materials and Pavement Design

Citation (APA)
Varveri, A., Jing, R., Tarsi, G., & Erkens, S. (2021). Effect of filler properties on the hydrothermal ageing of bituminous mastics. *Road Materials and Pavement Design*, *22*(S1), S2-S22. https://doi.org/10.1080/14680629.2021.1903975

Road Materials and Pavement Design

ISSN: (Print) (Online) Journal homepage: https://www.tandfonline.com/loi/trmp20

Effect of filler properties on the hydrothermal ageing of bituminous mastics

Aikaterini Varveri, Ruxin Jing, Giulia Tarsi & Sandra Erkens

To cite this article: Aikaterini Varveri, Ruxin Jing, Giulia Tarsi & Sandra Erkens (2021) Effect of filler properties on the hydrothermal ageing of bituminous mastics, Road Materials and Pavement Design, 22:sup1, S2-S22, DOI: 10.1080/14680629.2021.1903975

To link to this article: https://doi.org/10.1080/14680629.2021.1903975

Published online: 05 Apr 2021.

ROAD MATERIALS AND PAVEMENT DESIGN
2021, VOL. 22, NO. S1, S2–S22
https://doi.org/10.1080/14680629.2021.1903975

Taylor & Francis
Taylor & Francis Group

Effect of filler properties on the hydrothermal ageing of bituminous mastics

Aikaterini Varveri[a], Ruxin Jing [a], Giulia Tarsi[b] and Sandra Erkens [a]

[a]Department of Engineering Structures, Delft University of Technology, Delft, The Netherlands; [b]Department of Civil, Chemical, Environmental and Materials Engineering, University of Bologna, Bologna, Italy

ABSTRACT

Moisture sorption can significantly influence hydrothermal ageing and alter the chemical and rheological properties of bituminous mastics. Mineral filler particles are added to bituminous binders to form mastics with increased stiffness. The addition of fillers can considerably change the moisture sorption and the physico-chemical properties of binders by surface interactions and physical presence. This study aims to investigate the effect of filler type on the moisture-induced changes of bituminous mastics after wetting-drying cycles by means of sorption, rheological and infrared spectrometry tests. The results show that mineral fillers with higher diffusivity increase the overall capacity of mastics to absorb moisture, but at the same time allow for moisture desorption during drying. Nevertheless, it has been found that it is not the diffusivity properties but rather the bitumen and filler interactions that control the hydrothermal ageing of the mastics.

ARTICLE HISTORY
Received 7 September 2020
Accepted 12 March 2021

KEYWORDS
Bituminous mastics; moisture; wetting-drying cycles; mineral fillers; rheology; chemistry

Introduction

The presence of moisture can affect the mechanical performance of asphalt mixtures and decrease the overall loading capacity of pavement structures, having thus a critical effect on their durability and long-term performance (Airey & Choi, 2002; Apeagyei et al., 2014). This, in turn, results to higher costs for maintenance, repair and rehabilitation of road infrastructure systems (Varveri, Zhu et al., 2015).

Bitumen is used ubiquitously in paving materials and insulation industry because of its excellent adhesive properties, viscoelastic nature (flexibility), and hydrophobicity. Although bitumen is in its nature a waterproofing material, studies have demonstrated that it can uptake and retain moisture under normal atmospheric conditions (Cheng et al., 2003; Nguyen et al., 1992; Pettersson & Elert, 2001; Vasconcelos, 2010; Wei & Youtcheff, 2008). Moreover, the moisture sorption properties of bituminous binders can be significantly altered by the addition of mineral fillers, such as limestone, granite, or hydrated lime. Actually, fillers are intentionally added to bitumen in order to increase the stiffness and improve the fatigue life against permanent deformation of asphalt mixtures (Kassem et al., 2011). The presence of filler particles can alter the bitumen's microstructure, density, viscosity, and diffusivity characteristics. Mineral fillers have higher diffusion coefficients, compared to those of bitumen (Arambula et al., 2010; Cui et al., 2014; Kringos, 2007; Vasconcelos et al., 2010), and are expected to increase the moisture transport rates in bituminous mastics. The overall moisture sorption properties of bituminous mastics will, ultimately, depend on the filler type and content with increasing filler concentrations resulting in an increase in the moisture uptake rates (Kringos, 2007; Varveri, 2017).

CONTACT Ruxin Jing R.Jing@tudelft.nl

Earlier studies have been performed to investigate the effects of moisture on bituminous materials at various length scales. In asphalt mixtures, moisture was associated with reduced strength, stiffness and short fatigue life (Birgisson et al., 2005; Cheng et al., 2003; Collop et al., 2007; Lu & Harvey, 2006; Poulikakos & Partl, 2009; Varveri et al., 2016). The key factors that control moisture sensitivity are the air voids distribution and connectivity, the binder film thickness, aggregate type and mineral filler type (Arambula et al., 2007; Cheng et al., 2003; Kassem et al., 2011; Poulikakos & Partl, 2009; Varveri, Avgerinopoulos et al., 2015; Varveri et al., 2016). At mastic scale, the presence of moisture is also reported to result to strength degradation, fracture energy reduction and increased brittleness (Apeagyei et al., 2014; Kringos et al., 2011; Varveri & Scarpas, 2018). Nevertheless, bituminous mastics produced with fillers that have higher surface area and finer gradation were reported to have improved moisture sensitivity (Airey et al., 2008; Chaturabong & Bahia, 2018; Ekblad et al., 2015).

In most studies, the effect of mineral fillers on moisture sensitivity was investigated through mechanical tests by relating strength degradation with moisture conditioning time. This study aims to evaluate the effect of filler properties on the changes in chemistry and rheology of bituminous mastics due to hydrothermal ageing. A clear distinction between hydrothermal and oxidative ageing should be made. Hydrothermal ageing is related to the physical and chemical changes induced by water uptake in a bulk bituminous binder (or mastic). Ageing by water sorption in bituminous materials may then induce various effects: decrease in cohesive strength, plasticisation of the binders (or mastics) (Apeagyei et al., 2014), damage of bitumen/aggregate interface with debonding phenomena. On the other hand, oxidative ageing is caused by the interaction between the bitumen reactive components and the oxygen in air, which results in bitumen embrittlement (Makowska et al., 2017)

In this paper, the objective is to evaluate the rheological and chemical properties of bituminous mastics prepared with different filler types after hydrothermal ageing that involves wetting-drying cycles. Because the viscoelastic properties of mastics are controlled by the physico-chemical bitumen-filler interactions, an understanding of these interactions under moist conditions should provide the basis for understanding the durability of bituminous mastics and mixtures.

Materials and methods

Figure 1 illustrates the experimental methodology followed in this study. Details on the tested materials and the testing conditions can be found below.

Materials

Mineral fillers properties

The mineralogical compositions of mineral fillers are considered to have a profound influence on the evolution of damage due to hydrothermal ageing in bituminous mixtures (Kringos, 2007; Varveri, 2017) . In this study, four different fillers were employed including both commercial and non-commercial filler products. Wigro 60 K (WG 60 K) is a commercial filler supplied by Sibelco and consists of 75%wt. of limestone (calcium carbonate: CaCO3, category CC60), and 25%wt. of hydrated lime (calcium hydroxide $Ca(OH)_2$). This filler type is widely used in the Netherlands for the production of porous asphalt mixtures, due to the improved moisture sensitivity of asphalt mixtures. The second material used was a commercial quartz filler (QZ), the Silverbond M6 filler supplied by Sibelco, which is considered as a filler type of 'inert' nature; hence, it is anticipated that there will be no chemical interactions between the filler particles and the bitumen during hydrothermal ageing. Moreover, a Scottish granite filler (GR) to represent the acidic aggregates and a Norwegian sandstone (bestone) filler (BE) were adopted. The fillers were characterised in a previous study (Mastoras et al., n.d.) and their physical properties are summarised in Table 1.

The WG 60 K has the finest gradation (maximum particle size is 63 μm) followed by GR and BE, which have similar gradation, whereas QZ is the coarser filler (with a maximum particle size of 125 μm). From Table 1, it can also be seen that WG 60 K has the highest voids in the dry compacted fillers,

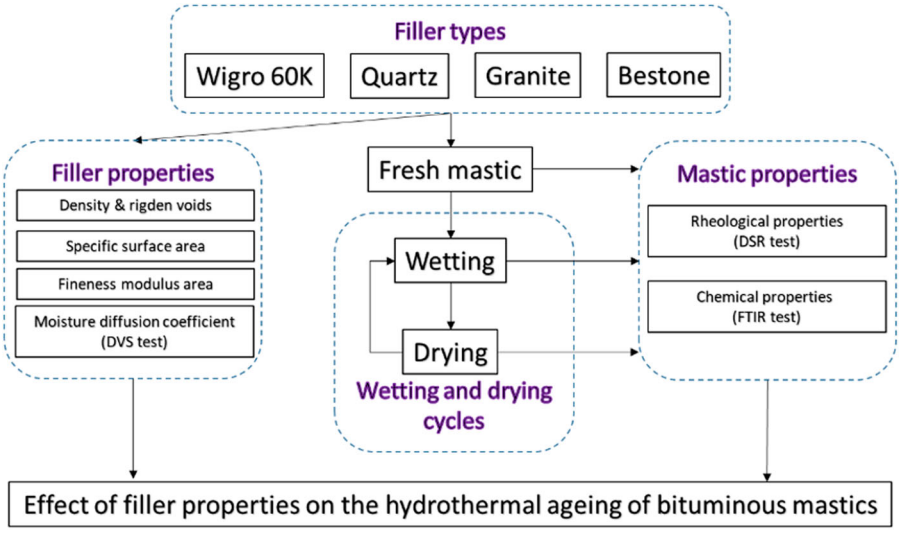

Figure 1. Experimental methodology.

Table 1. Physical properties of mineral fillers.

			Filler			
Property	Method	Units	Wigro60K [WG 60 K]	Quartz [QZ]	Granite [GR]	Bestone [BE]
Density	NEN-EN 1097–7	g/cm^3	2.54	2.64	2.64	2.70
Fineness modulus	–	–	2.32	4.67	3.44	3.55
Rigden voids	NEN-EN 1097–4	%	47.20	33.07	31.93	35.97
Specific surface area	Braunauer-Emmett-Teller (BET) method	m^2/g	8.51	0.80	3.03	2.01
Methylene blue	NEN-EN 933–9	g/kg	4.40	0.00	2.40	3.40
Particle size	BS ISO13320-1:1999	μm	1.0–63.0	1.0–125.0	1.0–90.0	1.0–90.0

or Rigden voids (RV) amongst all fillers, with BE, QZ, and GR fillers following in descending order of the RV values. The obtained RV values and their relation to the filler particles' size, distribution and surface texture are discussed elsewhere (Mastoras et al., n.d.). The specific surface area (SSA) of the fillers was determined using the Gemini VII 2390p surface area analyzer and the Braunauer–Emmett–Teller (BET) method. The WG 60 K filler has the largest SSA (8.51 m^2/g). The remainder fillers have quite smaller values of SSA, with the QZ filler exhibiting the smallest SSA that was measured equal to 0.80 m^2/g. The Methylene Blue test was also performed to determine harmful fines, such as clay and organic materials, in the mineral fillers. The presence of clay, such as montmorillonite, has been associated with water sensitivity of asphalt mixtures (Kandhal et al., 1998) due to the swelling properties of clays (Karpiński & Szkodo, 2015). WG 60 K shows the highest Methylene Blue value, which indicates the presence of clay and is followed by the BE and the GR fillers. The QZ filler does not have any harmful fines. Table 2 presents the mineralogy of the studied fillers determined using X-Ray diffraction analysis. The results show that all mineral fillers, apart from QZ, contain clay, namely mica and illite, as also indicated by the Methylene Blue test results.

The main minerals present in WG 60 K are calcite and dolomite that confirms the high calcium concentration, as shown in Table 3, where the elemental composition of the fillers is presented. On the other hand, QZ demonstrates a negligible calcium concentration, whereas the main element in this filler is the SiO2. Based on their SiO2 content (or based on their CaO content) the mineral fillers can be classified as acidic or basic (Nageswaran, 2016). The order of the studied fillers going from basic to acidic is: WG 60 K, BE, GR and QZ.

Table 2. Mineralogy of mineral fillers.

	Concentration (%)			
Mineral	WG 60K	QZ	GR	BE
Quartz	2.50	100.00	30.70	40.00
Plagioclase	–	–	40.20	17.80
K-Feldspar	2.50	–	21.00	7.20
Mica + Illite	7.00	–	2.10	15.80
Calcite	41.70	–	1.20	12.40
Chlorite	–	–	2.70	6.80
Pyroxene	–	–	2.10	–
Dolomite	17.30	–	–	–
Hematite	0.50	–	–	–
Portlandite	28.50	–	–	–

Table 3. Elemental composition of mineral fillers.

		Concentration (%)			
Oxide	Chemical formula	WG 60K	QZ	GR	BE
Iron	Fe_2O_3	1.193	0.034	1.958	3.711
Aluminium	Al_2O_3	2.933	0.150	14.485	11.533
Titanium	TiO_2	0.133	0.046	0.310	0.563
Potassium	K_2O	1.118	0.040	3.633	2.917
Calcium	CaO	49.510	0.026	2.015	8.657
Magnesium	MgO	3.950	0.008	0.720	2.266
Sodium	Na_2O	0.134	0.011	4.297	1.916
Silicon	SiO_2	9.960	99.571	70.719	60.716
Chromium	Cr_2O_3	–	0.001	0.012	0.016
Barium	BaO	0.009	0.004	0.127	0.087
Zirconium	ZrO_2	0.003	0.007	0.021	0.035
Strontium	SrO	0.044	–	0.046	0.049
LOI (%)		31.67	0.10	1.34	7.24

Bitumen and mastics: sample preparation

The mineral fillers were blended with a neat 40/60 penetration grade bitumen to produce the bituminous mastics. The bitumen was characterised by means of Penetration and Ring & Ball tests, according to the standards EN 1426 (2015a) and EN 1427 (2015b), respectively. The bitumen had a penetration value equal to 50.3 dmm, a softening temperature of 48.4°C and 1.03 g/cm^3 density.

The bituminous mastics were prepared with a filler-to-bitumen (f/b) ratio equal to 1 by weight. The sample preparation was performed according to the protocol developed by Mo (2010). The bitumen was scooped from its original storage can using a pre-heated knife at 150°C, so as to avoid multiple reheating cycles and avoid further ageing of the material. Both bitumen and filler were separately pre-heated in a forced air convection oven at 130°C for 1 h. The heating temperature and duration were selected following the standard EN 12594 (2014) with a final aim to guarantee a sufficient workability of bitumen and the removal of moisture from the mineral fillers. After heating up the materials, the filler was transferred into the bitumen can and the blend was manually stirred with a pre-heated spoon for 5 min. The blending phase was performed on a heating plate at 130°C to maintain a good workability of the bituminous mastic. To ensure that the filler particles fully interact with bitumen, both physically and chemically, the mastic samples were placed in the oven for 30 min. Because the filler particles tend to settle at the bottom of the can, the mastic samples were stirred again to ensure a good homogenisation before sampling. The bituminous mastics were poured into moulds to produce samples in a circular shape. Then, the filled moulds have been placed in the oven at 130°C for 10 min. This step is crucial to reduce or remove the air bubbles incorporated during the stirring phase. Finally, the samples were let to cool down at room temperature for 4 h and then to freeze at around −25°C

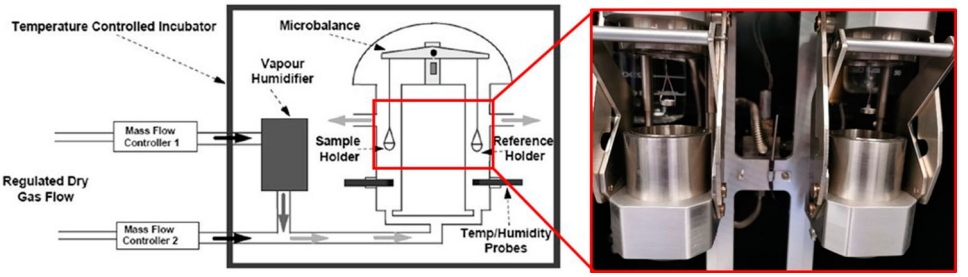

Figure 2. Operation principle of the Dynamic Vapour Sorption (DVS) device. (The image is reproduced with the permission of Surface Energy Measurement Systems, London, UK).

for 1.5 h. The same procedure was adopted for the preparation of the neat bitumen samples, without the addition of the mineral filler, to ensure a consistent thermal history for both mastics and bitumen.

Test methods

Hydrothermal ageing

The hydrothermal ageing protocol involved repeated wetting and drying cycles at a constant temperature. Specifically, the wetting phase of the mastics samples was performed by immersion of the samples in a water bath at a constant temperature of 30°C for 7 days; during the drying phase the samples were stored at ambient temperature and relative humidity (ca. 25°C and 60% RH) for 7 days after being removed from the water bath. The wetting-drying cycle was repeated three times, resulting in a total hydrothermal ageing time of 42 days. To avoid deformation, the samples were kept separately into aluminium containers, therefore water could diffuse only through the top surface of the samples. The chemical and rheological changes of the mastics were evaluated after each wetting and drying phase.

The protocol aimed to simulate local climate conditions. In the Netherlands, the yearly mean surface pavement temperature is 10°C, whereas the highest surface temperature in summer is about 30°C (Giezen et al., 2015). Moreover, rainfall is common throughout the year, which means there is no dry season per se but shorter wet and dry periods.

Moisture sorption tests

Hydrothermal ageing is strongly related to the moisture sorption properties of the mastics, namely the rate and amount of water absorbed into the bituminous matrix and the inorganic mineral fillers. In this study, one neat bitumen was blended with the filler phases using the same f/b ratio for all mastics. Hence, it is anticipated that the moisture sorption behaviour of the mastics will be primarily controlled by the sorption properties of the filler phase and its physico-chemical interactions with the bituminous matrix.

Moisture sorption experiments were performed by means of an automated gravimetric Dynamic Vapour Sorption (DVS) analyser. The operation principle of DVS is illustrated in Figure 2. The uptake of water vapour was determined gravimetrically using a high precision balance with a mass resolution of $\pm$0.1 µg. The relative humidity around the sample was controlled by mixing saturated and dry carrier gas streams using mass flow controllers. Prior to being exposed to water vapour, the filler samples were subjected to a drying stage (at 0% relative humidity) for a total of 4 h at 30°C to remove any moisture present. Next, the samples were exposed to a relative humidity (RH) of 95% at 30°C ($\pm$0.1°C) for 24 h (until they have reached moisture equilibrium) and the moisture uptake was measured.

Figure 3 shows typical gravimetric data for the sample moisture uptake at 95% RH and 30°C. Initially, during the drying phase, there is a decrease in mass with time due to the desorption of moisture from the sample. As indicated by the equilibrium mass reached by $t = 200$ min in Figure 3, the 240-minutes

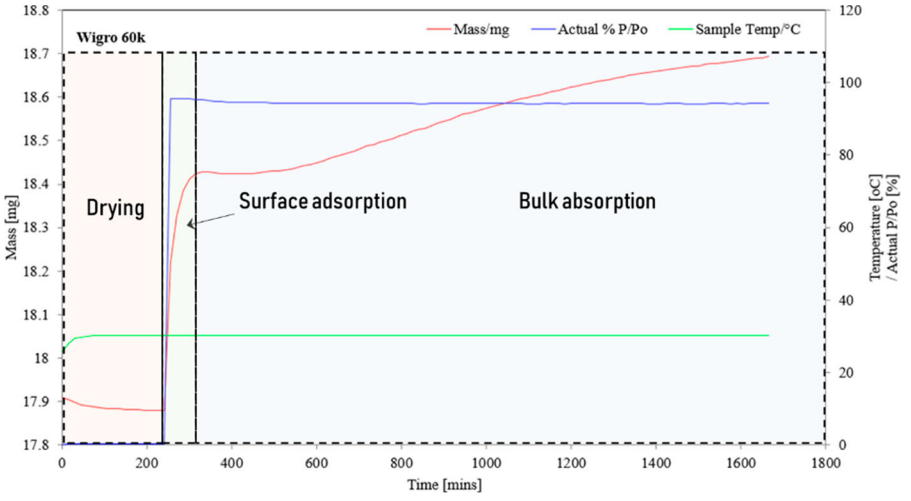

Figure 3. Kinetics of water sorption on the WG 60 K filler sample.

drying period was sufficient to completely dry the sample before exposing it to water vapour. As soon as moisture is introduced, a large increase in sample mass due to surface water adsorption is recorded and ends after 315 min, at which surface adsorption reaches an equilibrium state. After this initial surface adsorption, absorption into the bulk material phase occurs where the mass (M_t) increases in a slower rate compared to surface adsorption. After long-time exposure to the moisture vapour, bulk diffusion essentially ends and the sample is considered to have reached an equilibrium mass (M_{inf}).

The point (time, mass) at which the drying and the surface adsorption phases end (which is indicated by a change in the slope of the mass curve as shown in Figure 3) is initialised (set to $t = 0$ and $m = 0$) and assigned to be the starting point of moisture vapour diffusion (absorption) into the bulk.

The moisture absorption part of the sorption curve is used to calculate the diffusion coefficient (D). The moisture absorption data are fitted to the Fick's second law of diffusion, which can be used to describe non-steady mass transfer according to Equation (1).

$$\frac{\partial C}{\partial t} = D\frac{\partial^2 C}{\partial x^2} \tag{1}$$

Assuming a spherical geometry of the filler particles and a constant diffusivity, and considering a constant continuous source of moisture concentration, the following equation can be derived in spherical coordinates:

$$\frac{\partial C}{\partial r} = \frac{1}{r^2}\frac{\partial}{\partial r}\left(Dr^2\frac{\partial C}{\partial r}\right) \tag{2}$$

Solving the differential equation using the additional boundary condition of $dC/dr = 0$ at a radius of $r = 0$ (Crank, 1975), Equation (3), in which r_p is the filler particle radius, can be used to calculate the diffusion coefficient (D) of the mineral filler samples

$$\frac{M_t}{M_{inf}} = 1 - \frac{6}{\pi^2}\sum_{n=1}^{\infty}\frac{1}{n^2}\exp\left(-\frac{n^2\pi^2 Dt}{r_p^2}\right) \tag{3}$$

Dynamic shear rheometer testing

The effects of hydrothermal ageing on the rheological properties of the neat bitumen were evaluated by means of oscillatory tests.

The rheological behaviour of the mastics was investigated using an Anton Paar EC-Twist 502 rheometer, which is shown in Figure 4. At first, amplitude sweep tests were performed to determine

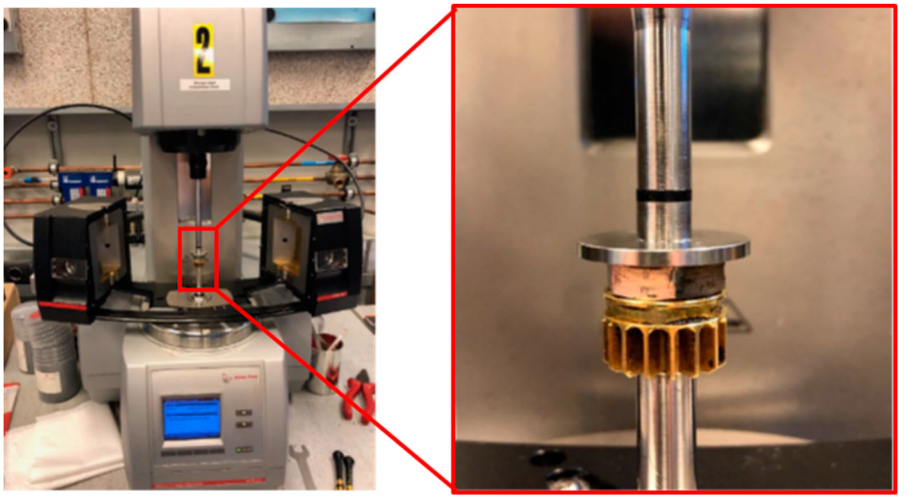

Figure 4. Dynamic shear rheometer.

the linear viscoelastic (LVE) limits, within which the complex shear modulus is relatively independent of the applied stress or strain. Consequently, the defined strains were used as the input testing parameters for the frequency sweep (FS) tests. The FS tests were performed in a stress-controlled mode using a parallel plate configuration, by applying an oscillatory sinusoidal load with variable testing frequencies from 0.2 to 20 Hz at six temperatures, namely −10, 0, 10, 20, 30 and 40°C. For the neat bitumen, an 8 mm plate (PP8) was used at test temperatures up to 20°C and a 25 mm plate (PP25) was used at higher temperatures. Due to the greater stiffness of mastics, the materials were tested with the PP8 configuration independent of the testing temperature.

The CAM model was used to describe the master curves for the complex shear modulus and phase angle using Equations (1) and (2). The change in the parameters of CAM model can be used to evaluate the influence of wetting-drying cycles on the rheological index IR of bitumen and mastics.

$$G^*(f) = G_g^*[1 + (f_p/f)^{\beta}]^{\alpha/\beta} \tag{4}$$

$$\delta(f) = \frac{90\alpha}{1 + (f/f_p)^{\beta}} \tag{5}$$

$$R = \frac{\log 2}{\beta} \tag{6}$$

where G_g^* is the glassy modulus, f_p is the position frequency at the cross point, α and β are the fitting parameters. All other model parameters can be obtained by minimising the mean relative error (MRE), as defined in Equation (4).

$$\text{MRE} = \sum \frac{|G^*_{\text{CAM}} - G^*_t|}{G^*_t} + \sum \frac{|\delta_{\text{CAM}} - \delta_t|}{\delta_t} \tag{7}$$

where G^*_{CAM} is the calculated value and G^*_t is the test value of the complex shear modulus, δ_{CAM} is the calculated value and δ_t is the test value of the phase angle.

Fourier transform infrared spectroscopy

Infrared spectroscopy provides information about the chemical functional groups of bituminous materials by means of the absorbed infrared radiation at a certain wavenumber range (Hofko et al., 2017). The Perkin Elmer Spectrum 100 FTIR spectrometer shown in Figure 5 was used in Attenuated Total Reflectance (ATR) mode, using a diamond crystal that is used to analyse a vast majority of sample types,

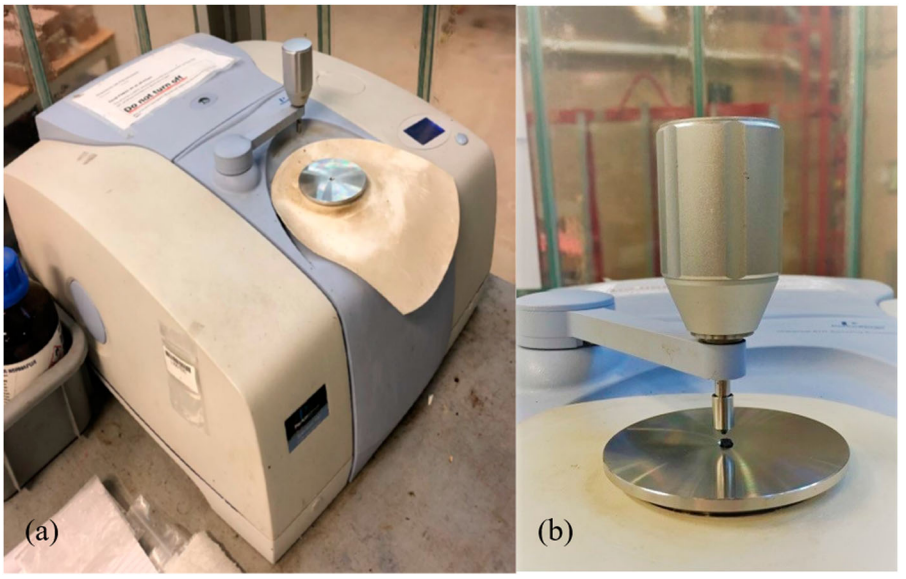

Figure 5. (a) FTIR spectrometer and (b) mastic sample on the crystal area of the FTIR-ATR top-plate.

i.e. liquids, powders or hard minerals. The FTIR spectra were collected at wavenumbers between 600 and 4000 cm^{-1}. Before testing, a background check was carried out automatically to define a relative scale for the absorption intensity. Ten replicates were tested for each analysed material in order to have a more reliable result. The samples underwent 20 scans with a scanning resolution of 4 cm^{-1} and the average value provide the final interferogram, which was then normalised on the basis of the asymmetric stretching vibration of the aliphatic structures at wavenumber equal to 2923 cm^{-1}. For normalisation, the absorbance value of this band was set to 1 and the complete spectrum was multiplied by a ratio factor.

The ageing indices and that one related to the presence of water (OH groups) were calculated using the integration of the area above the absolute baseline under specific wavenumber bandwidths over maximum peak-based methods (Hofko et al., 2017). The following equations were employed for the calculation of the carbonyl, sulfoxide and hydroxyl indices:

$$\text{Carbonyl} = \int_{1666}^{1746} a_{norm}(x)dx \tag{8}$$

$$\text{Sulfoxide} = \int_{924}^{1066} a_{\text{norm}}(x)dx \tag{9}$$

$$\text{Hydroxyl} = \int_{3000}^{3800} a_{\text{norm}}(x)dx \tag{10}$$

where $a_{\text{norm}}(x)$is the normalised absorbance value at wavenumber x.

Results and discussion

The effects of hydrothermal ageing on mastics, prepared by blending a neat bitumen with four different filler types to a constant f/b ratio, were evaluated from a rheological and chemical viewpoint. Also, the results of the sorption tests for the mineral fillers are reported.

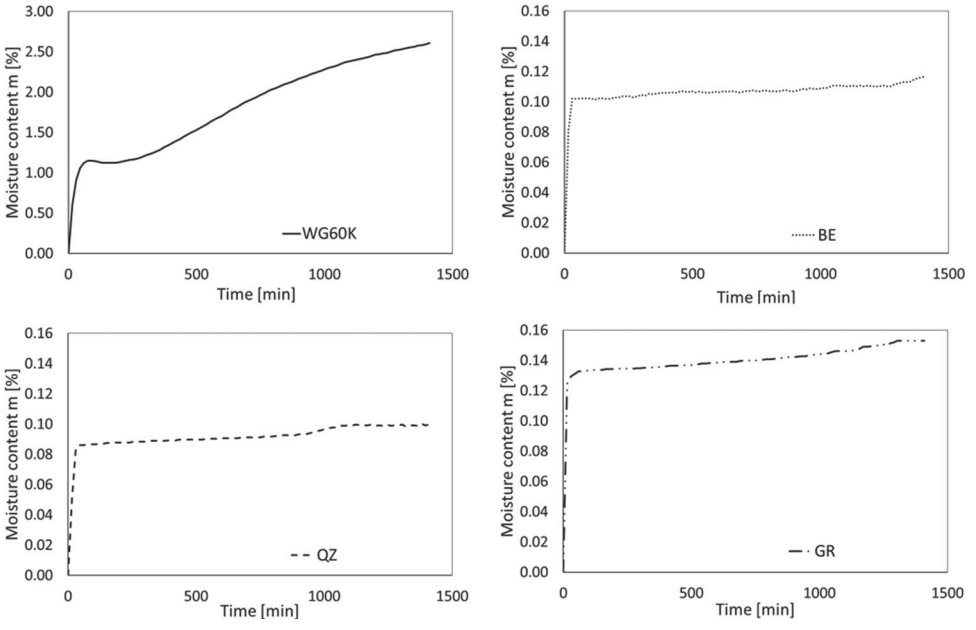

Figure 6. Normalised moisture content with time.

Moisture sorption behaviour of fillers

The normalised moisture content m was calculated using Equation (11), where w_t is the weight of the sample at each time t and w_o is the initial weight of the sample (actually the weight of the sample after the drying phase).

$$m\,[\%] = \frac{w_t - w_o}{w_o} * 100\% \tag{11}$$

The moisture content profiles are plotted against time in Figure 6 and reveal the differences in the rate and amount of moisture sorption for the studied mineral fillers. The initial slope of the sorption curves denotes the surface adsorption rate, whereas the slope of the second part of the curve denotes the bulk absorption rate.

It can be observed that the surface adsorption rate of fillers is higher for the WG 60 K filler, with the GR, BE and QZ fillers following in descending order. The observed adsorption behaviour can be explained by considering the specific surface area (SSA) values of the fillers. It can be hypothesised that a larger surface area essentially implies a higher number of adsorption sites on the surface of the filler particles for the water groups to bind. As shown in Table 2, WG 60 K has the highest SSA and the highest surface adsorption rate. On the contrary, QZ has the smallest SSA and shows the lowest absorption rate. For bulk absorption, WG 60 K shows the highest rate and amount of moisture absorption; the other three fillers exhibit similar absorption rates and moisture content. The rate and amount of moisture in the bulk of the fillers can be related to the Rigden voids (RV), which denotes higher porosity in the bulk filler material (as a percentage of the total volume of the filler) and could possibly lead to the absorption of higher moisture amounts. Indeed, the RV of the WG 60 K filler is equal to 47.20%, which is significantly higher than those of the QZ, GR, and BE fillers that have similar RV values (33.07%, 31.93%, and 35.97%, respectively). On the other hand, the high moisture content of WG 60 K might be due to the mineralogy of its particles, namely, the presence of calcite.

Plots of M_t/M_{inf} versus the square root of time for all filler types were produced for the bulk absorption part of the curve and then used to back-calculate the diffusion coefficients (Table 4) using Equation (3). The determination of the diffusion coefficient requires a narrow particle size range to

Table 4. Average particle radius and moisture diffusion coefficients of mineral fillers.

	Average particle radius r_p	Diffusion coefficient of moisture D
Filler type	μm	mm^2/s
WG 60K	2.05	6.72×10^{-5}
QZ	12.69	1.6×10^{-12}
GR	5.14	8.8×10^{-10}
BE	5.90	3.48×10^{-10}

ensure accurate and relevant results. Laser diffraction particle size analysis was performed for each filler type and the average particle radius (Table 4) was determined for each filler type based on its particle size distribution.

The values of the diffusion coefficients of the QZ, GR and BE fillers are found to be significantly lower in comparison to the value of WG 60 K. As discussed earlier, this difference can be explained by considering the physical fillers properties (SSA and RV) and the possible chemical interactions due to the mineralogical filler composition. The calculated diffusion coefficients for GR and BE are slightly lower than those of mineral aggregates reported in literature that range from 10^{-5}–10^{-9} mm^2/s (Cui et al., 2014; Kringos, 2007). This can be explained by the differences in the testing methods, the selected diffusion species and the testing conditions (such as temperature, humidity level) amongst the various studies. Moreover, the GR and BE fillers had a wide range of particle sizes and a coarse gradation which can lead to less accurate values when using the analytical solution in Equation (3).

Rheological properties

The master curves of the bituminous mastics at dry state and after hydrothermal ageing are presented in Figure 7. As a reference, the master curve of the neat bitumen is also added in the figure; the bitumen underwent the same thermal history as the bituminous mastics. In addition, Table 5 shows the CAM parameters for bitumen and mastics at different hydrothermal conditions. Major differences can be found between the complex modulus master curves of bitumen and mastics both at dry and conditioned states. In fact, it is known that filler causes an increase in the stiffness of the resulting mastics (Diab & Enieb, 2018), which is confirmed by the G_g values of bitumen and mastics in Table 5. Despite this general trend, greater differences can be observed at high frequencies and/or low temperatures. In this condition, bitumen exhibits a complex shear modulus of 10^8 Pa magnitude, while all other mastics tend asymptotically to the glassy state with a magnitude of 10^9 Pa.

It is evident that the type of mineral filler type influences the values of shear complex modulus, Figure 7(b). The use of WG 60 K filler leads to mastics with the highest stiffness, followed by the GR filler. On the other hand, the complex modulus of the QZ and BE mastics is similar to that of neat bitumen. Similar trends are observed for the phase angle master curves. The stiffness effect can be correlated with the physical properties of fillers (Aburkaba & Muniandy, 2016; EuLA, 2011).

The value of the rheological index R is associated with the relaxation spectrum. Higher values of R indicate a broader relaxation spectrum and a lower rate of the relaxation-induced decrease of the complex shear modulus. Table 5 shows that the addition of mineral fillers causes a reduction of the R index, indicating that the relaxation spectra narrows for the mastics, which implies that the material will have a faster stress relaxation. Analysis of the hydrothermal condition on different mastic indicates that hydrothermal ageing causes a decrease in the value of f_p, the position frequency at the cross point. The higher value of cross point of the viscous asymptote and glass modulus presents the less elasticity of the materials. Compared to their corresponding fresh (dry) state, the mastics become more elastic after hydrothermal ageing. The morphological parameters α and β do not change a lot at different hydrothermal conditions, which indicate that the master curves of mastics have similar shape and slope.

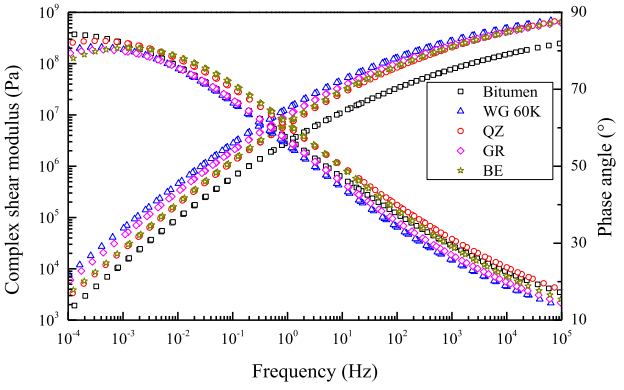

(a) Master curves of bitumen and mastics at dry state.

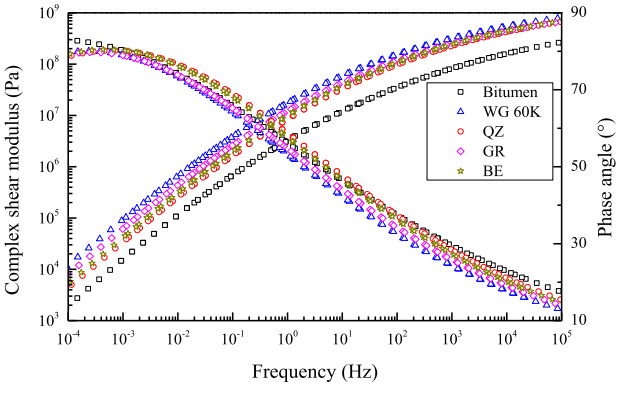

(b) Master curves of bitumen and mastics after three wetting-drying cycles.

Figure 7. Master curves of bitumen and mastics at different hydrothermal conditions.

Furthermore, to evaluate the four mastics with respect to their sensitivity to hydrothermal ageing, a sensitivity index is employed and calculated as the ratio of the crossover frequency at each conditioning state over the unconditioned state (original state before conditioning). The crossover frequency (crossover temperature) is used to characterise the viscoelastic fluid to solid transitory behaviour. As a result of ageing, the crossover frequency of bitumen normally decrease, which suggests that bitumen has longer relaxation time and higher softening point. The complex shear modulus corresponding to the crossover frequency is named crossover modulus. Moreover, the crossover modulus index was evaluated as well. The result of crossover frequency and modulus indices are reported in Figure 8.

There was no clear trend with respect to the changes in crossover modulus and frequency for the bitumen samples, as shown in Figure 8. On the other hand, it can be observed that all mastics have marginally lower crossover modulus and significantly lower crossover frequencies after the application of wetting-drying cycles. A comparison among the mastics suggests that WG 60 K mastic has the least changes in crossover modulus and frequency, which denotes lower hydrothermal ageing sensitivity.

To evaluate the effect of moisture diffusivity of fillers on the hydrothermal ageing behaviour of the mastics, the moisture diffusion coefficient of the fillers was plotted against the ratio of crossover frequency (modulus) after the three wetting-drying cycles in Figure 9. Considering that the mastics were prepared using the same base bitumen and that the filler content (by weight) was kept constant, it can be assumed that the apparent diffusivity of the mastics will be controlled by the diffusivity

Table 5. CAM model parameters of bitumen and mastics at different hydrothermal conditions.

Bitumen and mastic type	Condition	Parameters				Rheological index *R*
		α	β	G_g (GPa)	f_p (Hz)	
Bitumen	Fresh	−1.39	0.14	1.14	0.25	2.14
	1W	−1.37	0.14	1.16	0.40	2.12
	1D	−1.38	0.14	1.38	0.32	2.17
	2W	−1.40	0.14	1.44	0.18	2.23
	2D	−1.37	0.14	1.45	0.46	2.18
	3W	−1.39	0.13	1.49	0.22	2.23
	3D	−1.40	0.13	1.37	0.16	2.24
WG 60K	Fresh	−1.35	0.16	2.23	0.30	1.90
	1W	−1.34	0.16	2.21	0.29	1.88
	1D	−1.35	0.16	2.22	0.26	1.88
	2W	−1.36	0.16	2.30	0.22	1.92
	2D	−1.36	0.15	2.44	0.18	1.94
	3W	−1.38	0.15	2.37	0.14	1.96
	3D	−1.36	0.16	2.24	0.17	1.92
QZ	Fresh	−1.36	0.15	3.46	0.73	2.08
	1W	−1.30	0.16	2.38	1.22	1.91
	1D	−1.32	0.16	2.41	0.93	1.90
	2W	−1.31	0.16	2.28	0.96	1.90
	2D	−1.31	0.16	2.19	0.75	1.91
	3W	−1.32	0.15	2.45	0.68	1.96
	3D	−1.32	0.15	2.43	0.66	1.94
GR	Fresh	−1.34	0.16	2.10	0.38	1.94
	1W	−1.35	0.15	2.19	0.34	1.97
	1D	−1.33	0.16	2.09	0.35	1.93
	2W	−1.34	0.15	2.09	0.27	1.96
	2D	−1.34	0.15	2.26	0.27	1.99
	3W	−1.36	0.15	2.30	0.20	2.01
	3D	−1.35	0.15	2.16	0.23	1.97
BE	Fresh	−1.31	0.16	2.26	1.26	1.86
	1W	−1.35	0.15	3.58	0.75	2.05
	1D	−1.32	0.16	2.24	0.92	1.88
	2W	−1.33	0.16	2.30	0.68	1.93
	2D	−1.33	0.16	2.26	0.58	1.92
	3W	−1.32	0.16	2.07	0.66	1.88
	3D	−1.34	0.16	2.31	0.48	1.92

of each filler type. It is hypothesised that hydrothermal ageing will influence in a more severe degree the mastics with higher diffusivity. Interestingly, the results reveal that mastics prepared using mineral fillers with higher moisture diffusivity exhibit less changes in their crossover modulus, thus suggesting that they have better resistance to hydrothermal ageing. It can be suggested that there are two competing damage-inducing mechanisms that occur simultaneously, namely hydrothermal ageing and oxidative ageing. In mastics with high diffusivity moisture would quickly fill the voids and force the air out during hydrothermal ageing. This could slow down the oxidative ageing of the mastic, and could results in less changes in mastic stiffness within the specific conditioning time, as the hydrothermal ageing rate is normally lower than the oxidation rate (Huang et al., 2008).

Another hypothesis to explain this unforeseen relationship between mastic crossover modulus/frequency and filler diffusivity might be related to the physico-chemical bitumen-filler interactions. Intuitively, one would expect that it is the amount and the rate of moisture uptake that controls moisture sensitivity in bitumen-filler systems. Therefore, the physical presence of fillers with high porosity (RV) and diffusivity (diffusion coefficient) would be detrimental to the mastic properties. However, the results suggest that the mechanism related to the physical presence of the filler particles is not the dominant mechanism that affects hydrothermal ageing. The hydrothermal ageing

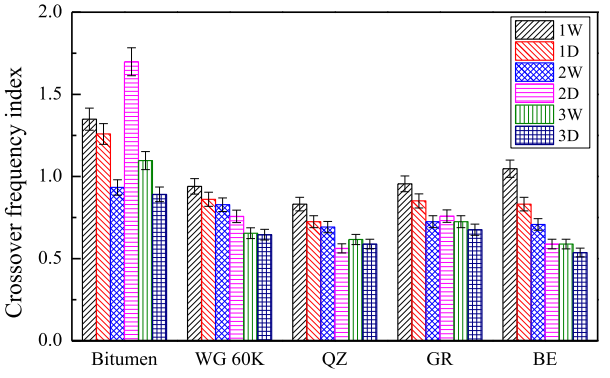

(a) Evolution of crossover frequency index with wetting-drying cycles.

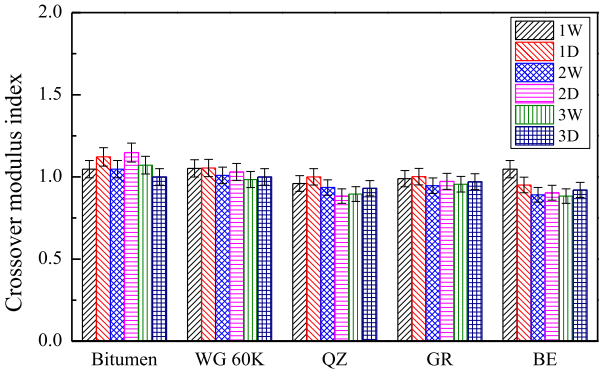

(b) Evolution of crossover modulus index with wetting-drying cycles.

Figure 8. Effect of wetting-drying cycles on crossover frequency and modulus indices.

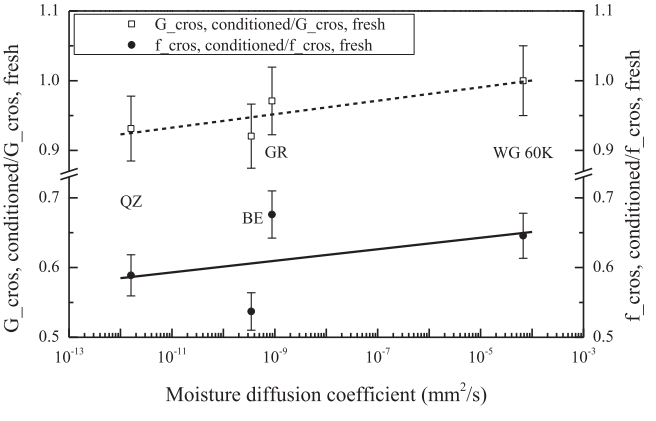

Figure 9. Change in crossover modulus (G_cros, conditioned/G_cros, fresh) and crossover frequency (f_cros, conditioned/f_cros, fresh) after three wetting-drying cycles versus the moisture diffusivity of fillers.

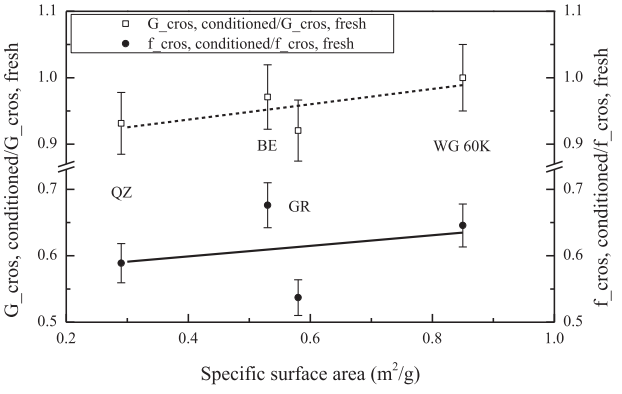

(a) Relation of crossover modulus and frequency and the filler surface area.

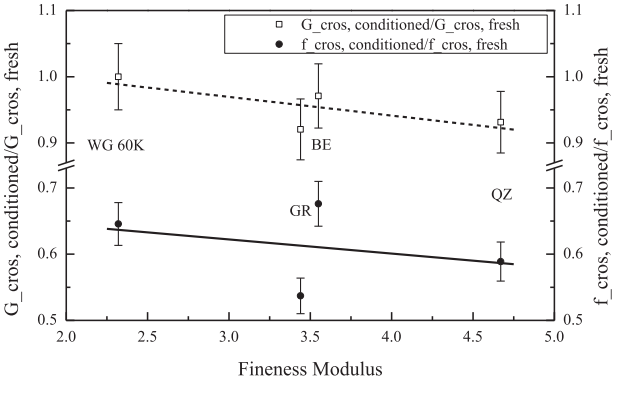

(b) Relation of crossover modulus and frequency and the fineness modulus.

Figure 10. Changes in crossover modulus and frequency after wetting-drying cycles and their relation to the physical properties of mineral fillers.

indices for crossover modulus and frequency were plotted against the SSA and fineness modulus of the corresponding fillers in Figure 10.

The results indicate that mastics produced using fillers with higher SSA and lower fineness modulus (hence with finer gradation) exhibit an improved hydrothermal ageing resistance. The WG 60 K filler has the highest SSA and lowest FM among the studied fillers and shows the lower hydrothermal ageing sensitivity. The use of WG 60 K filler, which contains calcium hydroxide $Ca(OH)_2$, is known for being an active filler that improves moisture resistance (Lesueur et al., 2013). On the other hand, the mastic with the highest hydrothermal sensitivity was found to be the mastic prepared with QZ filler that has the lowest SSA and the highest FM and is of inert nature. Therefore, it seems that mechanisms related to the interactions between bitumen and filler govern the hydrothermal ageing of mastics. However, the actual mechanisms are not yet understood and need to be further investigated.

Chemical properties

The ATR-FTIR spectra were collected at wavelengths between 600 and 4000 cm^{-1} in order to investigate the effects of hydrothermal ageing (wetting-drying cycles in the temperature range of 25–30°C)

Table 6. Mean, SD and SE values of the normalised areas in water region evaluated at different conditioning states.

Conditioning state	Bituminous materials	Mean value	SD	SE
Fresh	Bitumen	36.62	3.72	1.32
	WG 60K	46.21	4.41	1.56
	QZ	27.75	5.84	2.07
	GR	36.84	4.62	1.64
	BE	39.27	5.61	1.98
1W	Bitumen	37.76	2.88	1.02
	WG 60K	55.04	4.37	1.54
	QZ	32.68	4.46	1.57
	GR	33.50	3.13	1.11
	BE	40.11	4.68	1.65
1D	Bitumen	37.72	6.00	2.12
	WG 60K	39.66	1.92	0.68
	QZ	26.01	4.42	1.56
	GR	35.20	3.16	1.12
	BE	35.02	2.99	1.06
2W	Bitumen	39.59	5.49	1.94
	WG 60K	48.05	7.59	2.68
	QZ	27.33	4.05	1.43
	GR	39.38	7.08	2.50
	BE	46.65	3.22	1.14
2D	Bitumen	40.81	9.75	3.45
	WG 60K	43.17	2.28	0.80
	QZ	22.46	2.29	0.81
	GR	34.72	4.88	1.72
	BE	46.80	7.76	2.74
3W	Bitumen	42.47	6.41	2.27
	WG 60K	51.81	4.94	1.75
	QZ	34.45	5.53	1.96
	GR	45.92	5.80	2.05
	BE	48.12	6.11	2.16
3D	Bitumen	44.16	5.91	2.09
	WG 60K	45.40	3.95	1.40
	QZ	33.66	6.62	2.34
	GR	41.10	3.09	1.09
	BE	46.54	2.61	0.92

on the chemical composition of mastics. The absorption bands of the OH molecular vibrations (both symmetric and asymmetric stretch related to the presence of water) can be found at wavelength region of 3000–3800 cm^{-1} (Vasconcelos et al., 2011). The normalised peak areas at the above-mentioned wavelength region of water were evaluated at dry (fresh) state and after each wetting or drying phase according to Equation (10). The mean of normalised areas at the different conditioning states in the water absorption region (wavelengths of 3000–3800 cm^{-1}) for all bituminous materials are reported in Table 6, in addition the standard deviation (SD) and standard error (SE) values are listed.

The mean values of the integrated areas under the FTIR spectra exhibit the same order of magnitude regardless of the type of materials tested, i.e. bituminous binders or mastics. On the other hand, the SD and SE parameters allow the evaluation of the data variability. The collected data exhibits a not insignificant dispersion from the mean values; however, similar SD values were also found in previous spectroscopy analyses (Hofko et al., 2017), while the standard error values are lower than three (3), for most of the measurements with exception of those for standard bitumen after the drying phase of the second cycle.

The mean values of the Pen 40/60 bitumen sample show a gradual increase of the moisture area, albeit the increment was not constant per each phase of conditioning. This increasing trend implies that moisture could not be desorbed from bitumen during the drying phase. It can be

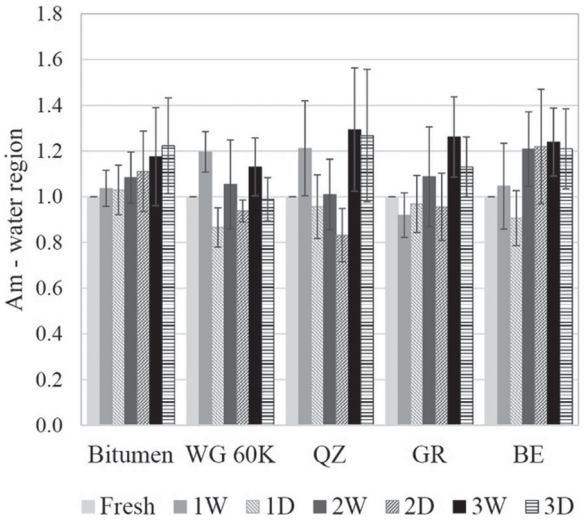

Figure 11. Calculated A_m areas of FTIR spectra in the water absorption region of bitumen and bituminous mastics at dry (fresh) state and after each wetting or drying phase.

therefore suggested that bitumen exhibits hysteretic effects with respect to the moisture absorption–desorption as the equilibrium moisture content was higher for the desorption (drying) cycle than for absorption (wetting). This finding corroborates the results of a previous study (Vasconcelos et al., 2011) in which existence of hysteresis of moisture diffusivity in three asphalt binders was observed. The cause of moisture history dependence still needs to be investigated and possibly linked to the changes in the bitumen chemical composition and microstructure at hydrothermal conditions. Conversely, the bituminous mastics show a clear absorption/desorption behaviour during the wetting-drying cycles. In order to highlight this behaviour, the normalised peak area ratio for moisture A_m was calculated according to Equation (12).

$$A_m = \frac{A_t}{A_o} \tag{12}$$

where $A_0$and $A_t$are the calculated areas for the water absorption region at dry conditions and after each cycle (wetting or drying), respectively. The A_m areas are plotted versus the conditioning state and the results are reported in Figure 11. The error bars represent a 95% confidence interval (CI).

As expected, the values of the normalised moisture area increase after the immersion of the materials in the water bath, while it decreases for all mastics after each drying cycle. The results suggest that the filler particles facilitate moisture transport, and at the same time, they also enable the release of moisture when the conditions are appropriate. The QZ and GR mastics do not show a significant moisture uptake during the first two wetting-drying cycles, as indicated by the growth of the moisture area (A_m). The presence of the QZ particles into the bitumen leads to a variable trend of the A_m ratio; it increases during the first wetting period and then decreases significantly, even becoming lower than unit during the second phase of conditioning, which denotes that the amount of moisture was less than in the dry case and it is not reasonable. After the third wetting phase moisture uptake (as expressed through A_m) increases significantly and the moisture area A_m reaches the highest value (> 1.3). The GR mastic experiences a first reduction in the water absorption area that has been detected by the instrument after the first wetting cycle. Then, the A_m value increases and exhibits the absorption/desorption behaviour in the following conditioning cycles. The particular results of both mastics during the first two wetting-drying cycles may be attributed to the variability of the FTIR test itself as shown in Figure 11 by means of error bars. The BE mastic experiences a lower moisture uptake after the first wetting phase compared to QZ and WG 60 K; while, it shows the highest A_m area during the

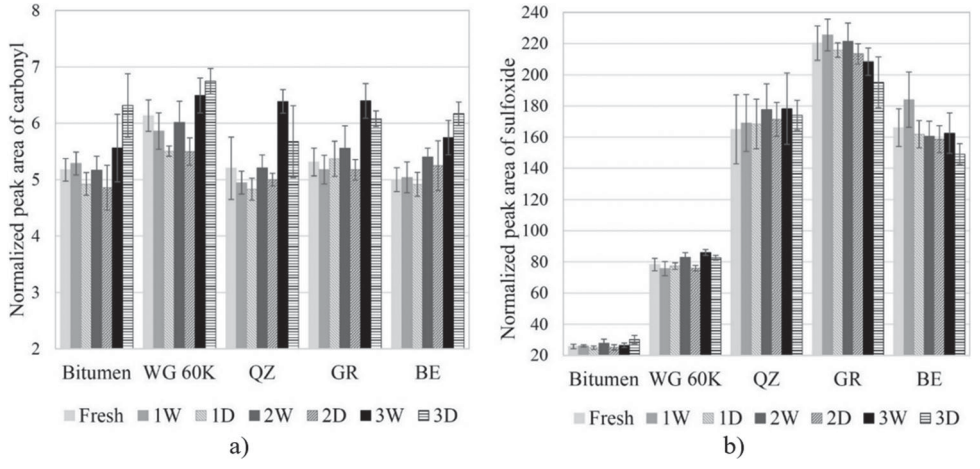

Figure 12. Average of normalised peak areas of the (a) C = O group and (b) S = O group of bitumen and bituminous mastics at fresh and after each wetting-drying cycles.

entire period of the second wetting phase. Overall, after the three wetting-drying cycles, the moisture uptake of the BE mastic is lower than that of the QZ mastic and neat Pen 40/60 bitumen; while it is higher than the uptake of WG 60 K and GR fillers. The WG 60 K mastic shows a clear absorption-desorption behaviour from the first wetting-drying cycle. The WG 60 K filler particles facilitate moisture uptake but also they easily allow for water adsorption as a consequence of the highest diffusion coefficient among all other mineral filler types. This behaviour can be related to the physical parameters of the WG 60 K filler since it has the highest SSA and RV among all studied mineral fillers. The QZ, BE and GR mastics have higher moisture uptake following in descending order at the end of the wetting-drying cycles; they appear not to be able to release moisture during the drying phases, which reflect their lower diffusivity than the WG 60 K filler.

The growth of the carbonyl (C = O) and sulfoxide (S = O) functional groups was analysed to estimate the hydrothermal ageing induced by the wetting-drying cycles. In detail, the carbonyl index was evaluated in the wavenumber band 1666–1746 cm^{-1}, while the sulfoxide index at wavenumbers between 924 and 1066 cm^{-1} (Hofko et al., 2017). The average of the integrated areas of FTIR spectra within the carbonyl and sulfoxide regions at dry and conditioned states is plotted against the conditioning phase in Figure 12.

The carbonyl area of neat bitumen and bituminous mastics (Figure 12(a)) is characterised by a lower variability after the first conditioning phases; then, the formation of C = O groups starts to be more variable, while their presence increases considerable at the third conditioning cycle. The growth of C = O functional groups is visible after the second wetting-drying cycle for BE and GR mastics especially; while it is still almost constant for the other mastics and bitumen. During the third wetting-drying cycle, the presence of carbonyl functional groups of bituminous materials follows two different trends. On one hand, the presence of carbonyls in neat bitumen, and BE and WG 60 K mastics increases regardless of the conditioning phase (wetting or drying). On the other hand, the evolution of the carbonyl functional group of the QZ and GR mastics differentiates from the other mastics after the second wetting-drying cycle; after this point, carbonyls increase after wetting and decrease after drying. Overall, the C = O groups show an increasing trend with wetting-drying cycles and the integrated areas under the spectra of all bituminous materials have a similar magnitude on average. These results suggest that bituminous materials experience oxidative ageing during the water conditioning even at relatively low temperature.

The growth of the S = O functional group at the considered experimental conditions is found to be less sensitive to hydrothermal ageing for the studied bituminous binder and mastics. Albeit, the

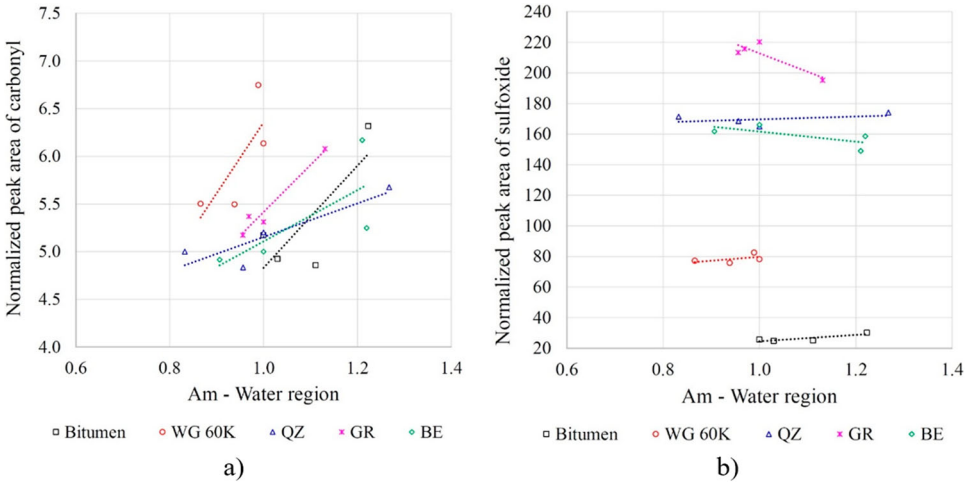

Figure 13. Evolution of the normalised peak areas of (a) carbonyl and (b) sulfoxide versus moisture content as expressed by the normalised peak area ratio A_m.

wetting-drying cycles lead to the increase of the S = O groups of the neat bitumen, the average areas under the FTIR sulfoxide peak showed a considerable lower magnitude than those of bituminous mastics. The evolution of the S = O bonds of bitumen has a similar behaviour as of the C = O one as it increases after the second wetting-drying cycle without showing any relation to the absorption/desorption phases, which is the case for the first two wetting-drying cycles (the area of S = O functional group increases with wetting and decreases with drying). On the other hand, the evolution of the S = O groups of the WG 60 K and QZ mastics follows the wetting-drying phases (thus the absorption-desorption behaviour). The increase or decrease in the sulfoxide group is related to the changes in the moisture content (as expressed through the A_m values). On the contrary, the S = O areas of the GR and BE mastics is relatively constant during the first two conditioning cycles and it decreases after being subjected to the three wetting-drying cycles. The bituminous mastics exhibit different absolute values of the sulfoxide functional groups. The presence of S = O groups is the highest in the GR mastics even at unconditioned state. While the introduction of WG 60 K filler leads to the lowest formation of the sulfoxide groups among all bituminous mastics.

In order to better comprehend the effect of the hydrothermal ageing, the indices of carbonyl and sulfoxide groups, which are usually used to evaluate oxidative ageing, are correlated with the A_m area ratios of moisture uptake. The evolution of the carbonyl and sulfoxide functional groups due to the hydrothermal ageing at fresh condition and after the drying phase of each cycle is reported in Figure 13.

The data indicate a direct tendency between the growth of carbonyl functional groups and moisture content. All studied mastics show an increasing trend of the C = O functional group with moisture. However, the trend lines of each mastic have different slope. The WG 60 K mastic presents the highest slope suggesting that this mastic experiences the lowest hydrothermal ageing. This behaviour corroborates the results of the rheological analysis as described earlier. Among all studied bitumen-filler systems, the QZ mastic has the lowest hydrothermal ageing resistance, which can be explained by the lower surface area and the chemical inert nature of the quartz filler. From Figure 13(b), there is no clear increasing tendency of the S = O groups and moisture uptake of bituminous materials. The data show higher variability for the various mastic types in terms of sulfoxide groups. The 40/60 bitumen and, WG 60 K and QZ mastics have a similar trend, where S = O bonds increase as the wetting-drying conditioning cycles increase. The GR and BE fillers allow the reduction of sulfoxide functional group

increasing the conditioning cycles. The use of WG 60 K mastic limits the development of S = O bonds due to the moisture uptake after wetting-drying cycles.

Summary and conclusions

The effect of four different types of mineral fillers on the hydrothermal ageing of bituminous mastics was investigated. Bitumen and mastics samples were subjected to wetting-drying cycles and their changes in rheology and chemistry were evaluated. Based on the experimental results the following conclusions can be drawn:

- Mineral fillers with fine gradation and high specific surface area have higher moisture sorption and uptake capacity.
- Mastics show a clear absorption-desorption behaviour during the wetting and drying cycles; in contrast, bitumen has a limited desorption capacity (within the limitations of this work) and suggests that there is a hysteresis between the moisture adsorption and desorption curves when subjected to cyclic conditioning.
- The rheological and chemical tests suggest that hydrothermal ageing is not primarily controlled by the diffusivity properties of the mineral fillers (and thus of the mastics), but the main mechanism relates to the bitumen-filler interactions. The sensitivity of mastics to hydrothermal ageing is less for mastics with fillers that have fine gradation, high specific surface area and are chemically active; albeit the use of these filler types results to mastics with higher diffusivity.

Acknowledgments

The authors are grateful to Mr Fabio Marchi for his help in the experimental testing of the bituminous mastic samples. Also, the authors would like to acknowledge Sibelco for providing the commercial fillers used in this study.

Disclosure statement

No potential conflict of interest was reported by the author(s).

ORCID

Ruxin Jing http://orcid.org/0000-0001-6975-807X
Sandra Erkens http://orcid.org/0000-0002-2465-7643

References

Aburkaba, E., & Muniandy, R. (2016). An overview of the use of mineral fillers in asphalt pavements. *Australian Journal of Basic and Applied Sciences*, *10*(May), 279–292.

Airey, G. D., & Choi, Y. K. (2002). State of the art report on moisture sensitivity test methods for bituminous pavement materials. *Road Materials and Pavement Design*, *3*(4), 355–372. https://doi.org/10.1080/14680629.2002.9689930

Airey, G. D., Collop, A. C., Zoorob, S. E., & Elliott, R. C. (2008). The influence of aggregate, filler and bitumen on asphalt mixture moisture damage. *Construction and Building Materials*, *22*(9), 2015–2024. https://doi.org/10.1016/j.conbuildmat.2007.07.009

Apeagyei, A. K., Grenfell, J. R. A., & Airey, G. D. (2014). Moisture-induced strength degradation of aggregate-asphalt mastic bonds. *Road Materials and Pavement Design*, *15*(S1), 239–262. https://doi.org/10.1080/14680629.2014.927951

Arambula, E., Caro, S., & Masad, E. (2010). Experimental measurement and numerical simulation of water vapor diffusion through asphalt pavement materials. *Journal of Materials in Civil Engineering*, *22*(6), 588–598. https://doi.org/10.1061/(ASCE)MT.1943-5533.0000059

Arambula, E., Masad, E., & Martin, E. (2007). Influence of air void distribution on the moisture susceptibility of asphalt mixes. *Journal of Materials in Civil Engineering*, *19*(8), 655–664. https://doi.org/10.1061/(ASCE)0899-1561(2007)19:8(655)

Birgisson, B., Roque, R., Tia, M., & Masad, E. (2005). *Development and evaluation of test methods to evaluate water damage and effectiveness of antistripping agents* (Final Report UF Project No.: 4910-4504-722-12). Florida Department of Transportation.

BSI Standards Publication. (2014). *Bitumen and bituminous binders – preparation of test samples*. Pub. L. No. 12594.

BSI Standards Publication. (2015a). *Bitumen and bituminous binders – determination of needle penetration*. Pub. L. No. 1426.

BSI Standards Publication. (2015b). *Bitumen and bituminous binders – Determination of the softening point – Ring and ball method.* Pub. L. No. 1427.

Chaturabong, P., & Bahia, H. U. (2018). Effect of moisture on the cohesion of asphalt mastics and bonding with surface of aggregates. *Road Materials and Pavement Design*, *19*(3), 741–753. https://doi.org/10.1080/14680629.2016.1267659

Cheng, D. X., Little, D. N., Lytton, R. L., & Holste, J. C. (2003). Moisture damage evaluation of asphalt mixtures by considering both moisture diffusion and repeated-load conditions. *Transportation Research Record: Journal of the Transportation Research Board*, *1832*(1), 42–49. https://doi.org/10.3141/1832-06

Collop, A. C., Choi, Y., & Airey, G. D. (2007). Effects of pressure and aging in SATS test. *Journal of Transportation Engineering*, *133*(11), 618–624. https://doi.org/10.1061/(ASCE)0733-947X(2007)133:11(618)

Crank, J. (1975). *The mathematics of diffusion* (2nd ed.). Clarendon Press.

Cui, S., Blackman, B. R. K., Kinloch, A. J., & Taylor, A. C. (2014). Durability of asphalt mixtures: Effect of aggregate type and adhesion promoters. *International Journal of Adhesion and Adhesives*, *54*, 100–111. https://doi.org/10.1016/j.ijadhadh.2014.05.009

Diab, A., & Enieb, M. (2018). Investigating influence of mineral filler at asphalt mixture and mastic scales. *International Journal of Pavement Research and Technology*, *11*(3), 213–224. https://doi.org/10.1016/j.ijprt.2017.10.008

Ekblad, J., Lundström, R., & Simonsen, E. (2015). Water susceptibility of asphalt mixtures as influenced by hydraulically active fillers. *Materials and Structures*, *48*(4), 1135–1147. https://doi.org/10.1617/s11527-013-0220-4

EuLA. (2011). *Hydrated lime: A proven additive for durable asphalt pavements – critical literature review* (Issue September).

Giezen, C., Mookhoek, S., & van Lent, D. (2015). *Field data of environmental impact* (Final Report of Ageing of Asphalt Pavements).

Hofko, B., Alavi, M. Z., Grothe, H., Jones, D., & Harvey, J. (2017). Repeatability and sensitivity of FTIR ATR spectral analysis methods for bituminous binders. *Materials and Structures/Materiaux et Constructions*, *50*, 187. https://doi.org/10.1617/s11527-017-1059-x

Huang, S. C., Turner, T. F., & Thomas, K. P. (2008). The influence of moisture on the aging characteristics of bitumen. *Proceedings of the 4th Eurasphalt and Eurobitume Congress* (p. 9).

Kandhal, P. S., Lynn, C. Y., & Parker, F. (1998). *Tests for plastic fines in aggregates related to stripping in asphalt paving mixtures* (Report No. 98-3). Auburn: National Center for Asphalt Technology.

Karpiński, B., & Szkodo, M. (2015). Clay minerals-mineralogy and phenomenon of clay swelling in oil&gas industry. *Advances in Materials Science*, *15*(43), 37–55. https://doi.org/10.1515/adms-2015-0006

Kassem, E., Masad, E., Lytton, R., & Chowdhury, A. (2011). Influence of air voids on mechanical properties of asphalt mixtures. *Road Materials and Pavement Design*, *12*(3), 493–524. https://doi.org/10.1080/14680629.2011.9695258

Kringos, N. (2007). *Modeling of combined physical-mechanical moisture induced damage in asphaltic mixes* [PhD Thesis, Delft University of Technology]. http://resolver.tudelft.nl/uuid:7d56c1e6-af8c-4a88-b7dc-2543b86279a2

Kringos, N., Khedoe, R., Scarpas, A., & de Bondt, A. (2011). A new asphalt concrete moisture susceptibility test methodology. *Transportation Research Board 90th Annual Meeting Compendium of Papers*.

Lesueur, D., Petit, J., & Ritter, H.-J. (2013). The mechanisms of hydrated lime modification of asphalt mixtures: A state-of-art review. *Road Materials and Pavement Design*, *14*(1), 1–16. https://doi.org/10.1080/14680629.2012.743669

Lu, Q., & Harvey, J. T. (2006). Evaluation of Hamburg wheel-tracking device test with laboratory and field performance data. *Transportation Research Record: Journal of the Transportation Research Board*, *1970*(1), 25–44. https://doi.org/10.1177/0361198106197000103

Makowska, M., Hartikainen, A., & Pellinen, T. (2017). The oxidation of bitumen witnessed in-situ by infrared spectroscopy. *Materials and Structures*, *50*(3), 1–17, article number 189. https://doi.org/10.1617/s11527-017-1058-y

Mastoras, F., Varveri, A., van Tooren, M., & Erkens, S. (n.d.). Effect of mineral fillers on ageing of bituminous mastics. *Construction and Building Materials*, *276*. https://doi.org/10.1016/j.conbuildmat.2020.122215

Mo, L. (2010). *Damage development in the adhesive zone and mortar of porous asphalt concrete* [Ph.D. thesis, Delft University of Technology]. http://resolver.tudelft.nl/uuid:968a9218-3a7d-4ec8-bfe8-156f2916000a

Nageswaran, P. D. C. (2016). Adhesion of aggregate-binder systems. [M.Sc. thesis, Delft University of Technology]. http://resolver.tudelft.nl/uuid:7e5631b8-4468-4f11-a9e6-f585209d94ad

Nguyen, T., Byrd, W. E., Bentz, D., & Seiler, J. (1992). Development of a technique for in situ measurement of water at the asphalt/model siliceous aggregate interface. In T. Nguyen, W. Eric Byrd, D. Bentz, & J. Seiler Jr. (Eds.), *SHRP-ID/UFR-92-611* (Vol. 501, pp. 1–56). National Research Council Washington DC.

Pettersson, M., & Elert, M. (2001). Charaterisation of bitumenised waste in SFR 1 – Report R-01-26. Swedish Nuclear Fuel and Waste Management Co. (Vol. R-01-26). https://doi.org/10.1007/s13398-014-0173-7.2

Poulikakos, L. D., & Partl, M. N. (2009). Evaluation of moisture susceptibility of porous asphalt concrete using water submersion fatigue tests. *Construction and Building Materials*, *23*(12), 3475–3484. https://doi.org/10.1016/j.conbuildmat.2009.08.016

Varveri, A. (2017). *Moisture damage susceptibility of asphalt mixtures experimental characterisation and modelling* [PhD Thesis, Delft University of Technology]. https://doi.org/10.4233/uuid

Varveri, A., Avgerinopoulos, S., Kasbergen, C., Scarpas, A., & Collop, A. (2015). Influence of air void content on moisture damage susceptibility of asphalt mixtures: A computational study. *Transportation Research Record: Journal of the Transportation Research Board*, *2446*(1), 8–16. https://doi.org/10.3141/2446-02

Varveri, A., Avgerinopoulos, S., & Scarpas, A. (2016). Experimental evaluation of long- and short-term moisture damage characteristics of asphalt mixtures. *Road Materials and Pavement Design*, *17*(1), 168–186. https://doi.org/10.1080/14680629.2015.1066705

Varveri, A., & Scarpas, A. (2018). Influence of moisture and freeze-thaw cycles on the cohesive properties of asphalt mortars. *Transportation Research Board 97th Annual Meeting Compendium of Papers*.

Varveri, A., Zhu, J., & Kringos, N. (2015). Moisture damage in asphaltic mixtures. In *Advances in asphalt materials: Road and pavement construction*. Elsevier Ltd. https://doi.org/10.1016/B978-0-08-100269-8.00010-6

Vasconcelos, K. L. (2010). *Moisture diffusion in asphalt binders and fine aggregate mixtures* [PhD thesis, Texas A&M University]. http://hdl.handle.net/1969.1/ETD-TAMU-2010-05-7651

Vasconcelos, K. L., Bhasin, A., & Little, D. N. (2010). Measurement of water diffusion in asphalt binders using Fourier transform infrared–attenuated total reflectance. *Transportation Research Record: Journal of the Transportation Research Board*, *2179*(1), 29–38. https://doi.org/10.3141/2179-04

Vasconcelos, K. L., Bhasin, A., & Little, D. N. (2011). History dependence of water diffusion in asphalt binders. *International Journal of Pavement Engineering*, *12*(5), 497–506. https://doi.org/10.1080/10298436.2010.535536

Wei, J., & Youtcheff, J. (2008). *Ongoing research to determine moisture diffusion coefficients of asphalt binders*. Internal Rep. Federal Highway Administration.